IJMMM International Journal of Minerals, Metallurgy and Materials 矿物冶金与材料学报（英文版）

A novel fluorescence turn-on sensor for Cr^{3+} based on fluorescence resonance energy transfer between gold nanoparticles and rhodamine B

Qin Ma, Lin Shi, Baocheng Ran, Tianfeng Ma, Huan Wang, and Yongchang Lu

Cite this article as:
Qin Ma, Lin Shi, Baocheng Ran, Tianfeng Ma, Huan Wang, and Yongchang Lu, A novel fluorescence turn-on sensor for Cr^{3+} based on fluorescence resonance energy transfer between gold nanoparticles and rhodamine B, *Int. J. Miner. Metall. Mater.*, 32(2025), No. 7, pp. 1762-1770. https://doi.org/10.1007/s12613-024-3010-9

View the article online at SpringerLink or IJMMM Webpage.

Articles you may be interested in

Fangyi Zhao, Zhen Song, and Quanlin Liu, Novel Cr^{3+}-activated far-red emitting phosphors with -$Ca_3(PO_4)_2$-type structure for indoor plant cultivation, *Int. J. Miner. Metall. Mater.*, 29(2022), No. 6, pp. 1286-1294. https://doi.org/10.1007/s12613-021-2363-6

Yue Liu, Shaobo Huang, Shanlong Peng, Heng Zhang, Lifan Wang, and Xindong Wang, Novel Au nanoparticles-inlaid titanium paper for PEM water electrolysis with enhanced interfacial electrical conductivity, *Int. J. Miner. Metall. Mater.*, 29(2022), No. 5, pp. 1090-1098. https://doi.org/10.1007/s12613-022-2452-1

Qiang Ge, Wen-hui Kong, Xin-qian Liu, Ying-min Wang, Li-feng Wang, Ning Ma, and Yan Li, Hydroxylated graphene quantum dots as fluorescent probes for sensitive detection of metal ions, *Int. J. Miner. Metall. Mater.*, 27(2020), No. 1, pp. 91-99. https://doi.org/10.1007/s12613-019-1908-4

Natpichan Pienutsa, Krittamet Yannawibut, Jetthana Phattharaphongmanee, Oukrit Thonganantakul, and Sira Srinives, Titanium dioxide-graphene composite electrochemical sensor for detection of hexavalent chromium, *Int. J. Miner. Metall. Mater.*, 29(2022), No. 3, pp. 529-535. https://doi.org/10.1007/s12613-021-2338-7

Dan Han, Xiaoru Liu, Donghui Li, Jiexu Shi, Yu Wang, Yuxuan Wang, Hongtao Wang, and Shengbo Sang, NO_2 gas sensor with high selectivity and fast response based on Pt-loaded nanoporous GaN, *Int. J. Miner. Metall. Mater.*, 32(2025), No. 4, pp. 964-972. https://doi.org/10.1007/s12613-024-2959-8

Chao Tan, Junling Lü, Chunchi Zhang, Dong Liang, Lei Yang, and Zegao Wang, Force and impulse multi-sensor based on flexible gate dielectric field effect transistor, *Int. J. Miner. Metall. Mater.*, 32(2025), No. 1, pp. 214-220. https://doi.org/10.1007/s12613-024-2968-7

IJMMM WeChat

QQ author group

INTERNATIONAL JOURNAL OF
Minerals, Metallurgy and Materials

Volume 32, Number 7, July 2025
Page 1762

Research Article https://doi.org/10.1007/s12613-024-3010-9

A novel fluorescence turn-on sensor for Cr^{3+} based on fluorescence resonance energy transfer between gold nanoparticles and rhodamine B

Qin Ma[1)], *Lin Shi*[2,4)], *Baocheng Ran*[3)], *Tianfeng Ma*[2,4)], *Huan Wang*[2,4),✉], *and Yongchang Lu*[2,4),✉]

1) Instrumental Analysis Center of Laboratory and Equipment Management Department, Qinghai Minzu University, Xining 810007, China
2) Modern Tibetan Medicine Creation Engineering Technology Research Center of Qinghai Province, Xining 810007, China
3) College of Chemistry and Materials Science, Qinghai Minzu University, Xining 810007, China
4) College of Pharmacy, Qinghai Minzu University, Xining 810007, China
(Received: 7 June 2024; revised: 1 September 2024; accepted: 11 September 2024)

Abstract: Up to now, "Turn-on" fluorescence sensor exhibits promising potential toward the detection of heavy metal ions, anions, drugs, organic dyes, DNA, pesticides, and other amino acids due to their simple, quick detection, and high sensitivity and selectivity. Herein, a novel fluorescence method of detecting Cr^{3+} in an aqueous solution was described based on the fluorescence resonance energy transfer between rhodamine B (RhB) and gold nanoparticles (AuNPs). The fluorescence of RhB solution could be obviously quenched ("off" state) with the presence of citrate-stabilized AuNPs. However, upon addition of Cr^{3+} to AuNPs@RhB system, the fluorescence of AuNPs was recovered owing to the strong interaction between Cr^{3+} and the specific groups on the surface of citrate-stabilized AuNPs, which will lead to the aggregation of AuNPs ("on" state). At this point, the color of the reaction solution turned to black. Under optimal conditions, the limit of detection (LOD) for Cr^{3+} was 0.95 nM (signal-to-noise ratio, S/N = 3) with a linear range of 0.164 nM to 3.270 μM. Furthermore, the proposed method exhibits excellent performances, such as rapid analysis, high sensitivity, extraordinary selectivity, easy preparation, switch-on fluorescence response, and non-time consuming.

Keywords: switch-on fluorescence response; gold nanoparticles; rhodamine B; trivalent chromium ion; fluorescence resonance energy transfer

1. Introduction

Recently, owing to the rapid development of industries such as textile, plastic, paper, leather, and food processing, various pollutants like antibiotics, toxic dyes [1–4], and heavy metal ions were released into the ecosystem and threatened the survival of human [5–7]. Among them, heavy metal ions like trivalent chromium ion (Cr^{3+}) have received significant attention [8–10]. We all known that chromium ion (Cr^{3+}), which is an essential trace element, plays a significant role in environment and biological process [11–12]. This important metal ion is closely related with the physiological activities of cells such as metabolism of fats, carbohydrates, and proteins [13–14]. Nevertheless, an overdose of Cr^{3+} can cause the genotoxic effect and malignant cancer [15–16]. Conversely, Cr^{3+} deficiency may lead to nervous system disorder, diabetes, and cardiovascular diseases [17–18]. Consequently, it is critical to develop a rapid, efficient, and highly selective analysis method to monitor of Cr^{3+} for environmental and human health.

Until now, several *in vitro* and *in vivo* analytical methods have been reported for detecting Cr^{3+}, including high-performance liquid chromatography (HPLC), atomic absorption spectrometry (AAS), ion-coupled plasma-mass spectroscopy (ICP-MS), electrochemical analysis [19], colorimetric sensor [20–21], and liquid chromatography with ultraviolet detection (LC-UV). Despite the mentioned methods were widely used in the field of food and drug analysis, they have major disadvantages such as most of them are usually require extensive sample purification, expensive instrumentation, poor interference immunity, complexity, and the need for special equipment. In contrast, fluorescence analysis is a promising method for detection of Cr^{3+} due to its advantages of low-cost, real-time detection, simplicity, and high sensitivity.

Interestingly, nanoparticles, especially gold nanoparticles (AuNPs), have been broadly utilized to the fields of molecular recognition, sensor [22–23], photocatalysis [24], electrochemiluminescence (ECL), and fluorescence analysis, due to its unique advantages of instinct optical properties, extremely high extinction coefficient, strong surface plasmon resonance (SPR), and color-tunable optical properties [25–27]. Furthermore, the easy-to-modify surfaces of AuNPs have been successfully utilized as color reporters for colorimetric cartap sensing a large variety of targets. Therefore, AuNPs have been used as ideal color reporters for colorimet-

✉ Corresponding authors: Huan Wang E-mail: qhmuwh1028@126.com; Yongchang Lu E-mail: qhlych@126.com
© University of Science and Technology Beijing 2025

ric sensors. At the same time, the fluorescence analysis method based on AuNPs have been widely applied in the detection of heavy metal ions, anions, proteins, organic molecules, etc. [28]. For example, Zhang *et al.* [29] reported an electrochemical-based nonenzymatic detection of glucose by using dendrimer-coated AuNPs via water splitting-assisted electrocatalysis. Based on gold nanoparticles capped with orthohydroxybenzoic acid, Andreani *et al.* [30] established a fast and selective colorimetric detection of Fe^{3+}. Zhao *et al.* [31] used the AuNPs/TiO_2 composites for remarkably enhanced photocatalytic H_2 evolution. Sun *et al.* [32] designed a simple colorimetric and fluorescent "on-off-on" dual-mode sensor based on cyan fluorescent carbon dots (G-CDs)/AuNPs system to detect L-cysteine and zinc thiazole. Xiong *et al.* [33] proposed an ECL immunosensor based on localized surface plasmon resonance (LSPR) between AuNPs and polymer dots (Pdots) for the determination of pancreatic cancer exosomes, and Wang *et al.* [34] developed a urinary miRNA ultratrace detection strategy based on single-target DNA-functionalized AuNPs for the noninvasive prognosis of post-myocardial infarction (post-MI). However, there is no report on the determination of Cr^{3+} through the change of fluorescent intensity and color based on the fluorescence resonance energy transfer between gold nanoparticles (AuNPs) and rhodamine B (RhB).

Herein, a switch-on fluorescent sensor was described for highly selective and sensitive detection of Cr^{3+} based on recovered fluorescence (FL) intensity of AuNPs@RhB system. The sensing mechanism is illustrated in Fig. 1. Firstly, the AuNPs@RhB fluorescent probe was prepared based on the fluorescence resonance energy transfer (FRET) between AuNPs and RhB, resulting the weak fluorescence emission of RhB ("off" state). Interestingly, the fluorescence of AuNPs@RhB system was recovered by Cr^{3+}, which interacted with Cr^{3+} to recover the quenched fluorescence due to the complexation between the specific groups on the surface of citrate-stabilized AuNPs and Cr^{3+} ("on" state). Thus, a rapid and strong selectivity RhB based "Turn-on" fluorescent sensor for Cr^{3+} was constructed and successfully applied to the detection of Cr^{3+} in actual samples. Finally, the simple method has advantages of safety, rapid, high efficiency sensitivity, and low cost.

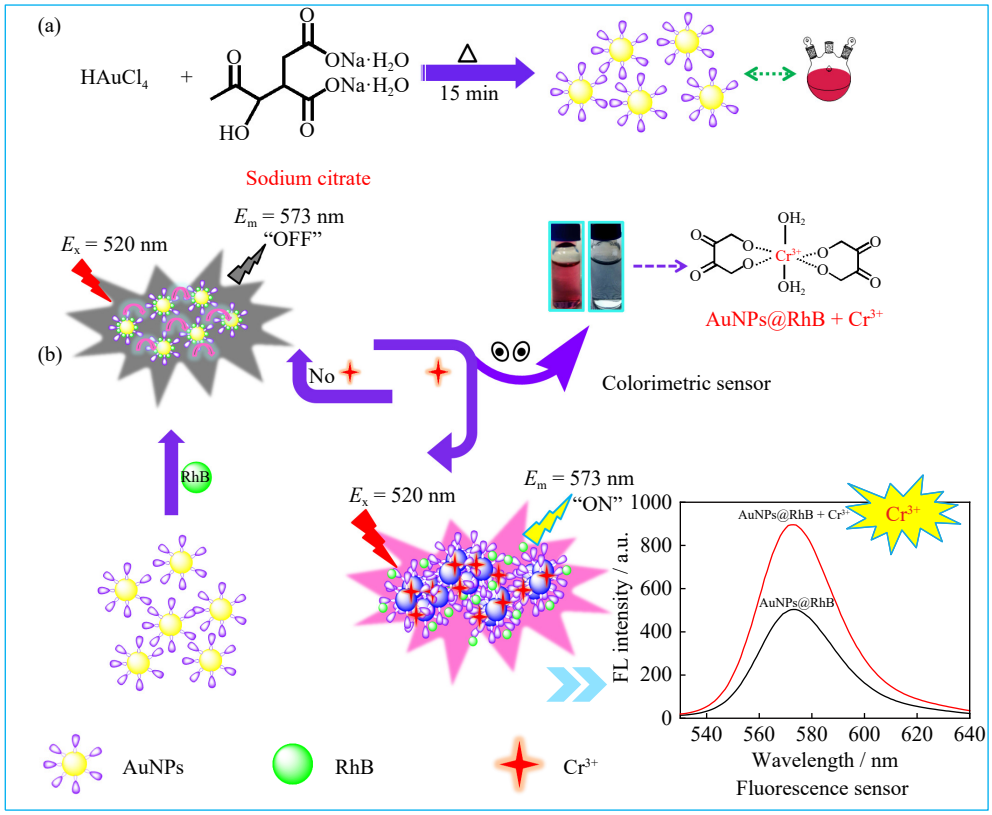

Fig. 1. (a) Schematic illustration of the fabrication process of the AuNPs. (b) Schematic illustration of Cr^{3+} detection using AuNPs@RhB system as the fluorescence probe and colorimetric sensor. E_m and E_x denote emission wavelength and excitation wavelength, respectively.

2. Experimental

2.1. Materials

Chloroauric acid ($HAuCl_4 \cdot 3H_2O$, ≥99.9%) and chromic nitrate ($Cr(NO_3)_3$) were purchased from Aladdin Chemical Reagent Co. (Shanghai, China); trisodium citrate ($C_6H_5Na_3O_7 \cdot 2H_2O$, 98%) was obtained from Sinopharm Chemical Reagent Co., Ltd.; trihydroxymethylaminomethane (Tris, 98%), NaOH, KCl, and other nitrates were purchased from Tianjin Kaixin Chemical Co. Ltd., (Tianjin, China). All chemicals were analytical reagent grade and used without further purification. Ultrapure water was used in all experiments.

2.2. Apparatus and characterization

Fluorescent emission spectra were recorded on the Cary Eclipse Fluorescence Analyzer (RF-5301PC, Shimadu Co., Japan). A UV-2450PC double-beam UV–vis spectrophotometer (Shimadu Co., Japan) was used to record absorption spectra. Fourier transform infrared spectrometer (FT-IR, Nicolet Instrument Co. Madison, WI, USA) were performed to determine the chemical structure of the samples. The pH value of the buffer solution was tested using the PHS-3B pH meter (Shanghai Instrument Co. Ltd., Shanghai, China).

2.3. Synthesis of citrate-stabilized gold nanoparticles

The citrate-stabilized AuNPs was prepared via a simple chemical reduction process, as illustrated in Fig. 1(a). In the beginning of preparation of AuNPs, all the glassware must be systematically cleaned with freshly prepared aqua regia (3:1, volume ratio of HCl : HNO_3) for about 24 h and washed carefully with double distilled water. Then, the AuNPs was prepared by the reduction of $HAuCl_4$ with trisodium citrate ($C_6H_5Na_3O_7{\cdot}2H_2O$) according to previous literature [35]. In brief, 1vol% $HAuCl_4$ (1 mL, 10 mg·mL^{-1}) solution was added to deionized water (100 mL) and heated to boil. After that, 10 mL (38.3 mM) fresh trisodium citrate solution was rapidly poured into the boiling $HAuCl_4$ solution and unceasingly heated for about 15 min, followed by vigorous stirring to produce wine-red coloured solution. Finally, the gold colloidal solution was cooled to room temperature and kept in a refrigerator at 4°C before using.

2.4. Preparation of solutions

The Tris–HCl buffer solution was used to investigate the influence of pH on the measurements of Cr^{3+}. Firstly, it was necessary to prepare 100 mL (0.10 M) Tris solution and 100 mL (0.10 M) HCl solution. Then, the different pH values were measured by pH meter based on continuously adjusting the volume ratio of the above solutions. Therefore, a pH = 6 Tris–HCl buffer solution was prepared.

2.5. Fluorescence detection of Cr^{3+}

The fluorescence sensor for Cr^{3+} detection was processed at room temperature in a Tris–HCl (pH = 6) buffer solution. AuNPs (800 μL, 3 nM) was added to the solution containing RhB (1.015 mL, 1.5 μM) and Tris–HCl (1.1 mL, 0.01 M, pH = 6) buffer solution, shaking thoroughly and keeping for 2 min. Next, different concentrations of Cr^{3+} were injected into the mixture. After incubation for about 7 min, the fluorescent intensity of AuNPs@RhB system in the presence (F) and absence (F_0) of Cr^{3+} were recorded at the 520 nm excitation wavelength and the 573 nm emission wavelength, and both excitation and emission slits were set at 5 nm with 530–650 nm wavelength scan range.

2.6. Selectivity measurements of Cr^{3+}

In the selectiviormaty test of Cr^{3+}, various metal ions (Al^{3+}, Na^+, Ca^{2+}, Pb^{2+}, Mg^{2+}, Ni^{2+}, Hg^{2+}, K^+, Fe^{3+}, Zn^{2+}, Mn^{2+}, Cr^{6+}, Ag^+, Cu^{2+}, Co^{2+}, Cd^{2+}, and NH_4^+) were selected as the coexisting substances in the investigation of Cr^{3+} by the AuNPs@RhB system under optimal conditions. The excitation wavelength was 520 nm and the emission wavelength was 573 nm under the condition of both excitation and emission slits set at 5 nm with 530–650 nm wavelength scan range.

2.7. Fluorescence sensor detection of Cr^{3+} in real samples

To prove the detection perfnce of this method in practical application, the river water was centrifuged at 10000 r/min for 10 min and the supernatant was collected. Then, the real samples were diluted to appropriate concentration in the detection range using ultrapure water, and stored in a refrigerator at 4°C. Subsequently, the detection of Cr^{3+} was tested by standard addition method, and the concentration of Cr^{3+} was determined according to the proposed method.

3. Results and discussion

3.1. Synthesis of citrate-stabilized gold nanoparticles

The morphology and dispersity of the obtained AuNPs by transmission electron microscopy (TEM) were shown in Fig. 2(a)–(b). The results proved that the obtained AuNPs was spherical in shaped and homogeneously dispersed in aqueous solution with an average size of 13.3 nm. In addition, the optical property of citrate-stabilized AuNPs was characterized by UV–vis absorption spectrum in the wavelength range of 320 to 700 nm. As depicted in Fig. 2(c), a strong characteristic surface plasmon resonance (SPR) peak around 522 nm was observed, which could be utilized to gain the concentration of AuNPs solution according to Lambert-Beer's law. According to the previous report [36], the extinction coefficient was 2.7×10^8 M^{-1}·cm^{-1} for the AuNPs. Therefore, the concentration of AuNPs solution was calculated to be 14.5 nM. In addition, Fig. 2(d) displays the zeta potentials of AuNPs in the different pH values. The results showed that the zeta potentials were about −14, −18, −22.1, −26.6, and −32.1 mV at pH 5.0, 6.0, 7.0, 8.0, and 9.0, respectively, which means that the zeta potential of the prepared gold nanoparticles becomes more negative with the increase of pH value.

3.2. Optimization of detection conditions

In order to obtain high detection sensitivity, several related experimental conditions, such as the concentration of RhB ([RhB]), the incubation time, and the medium pH value, were discussed. Firstly, the concentrations of RhB played an important role for the detection of Cr^{3+} in this work. As shown in Fig. 3(a), it was found that the fluorescence intensity of RhB solution trended to a maximum value when the RhB concentration was about 0.52 μM. Therefore, 0.52 μM was chosen as the typical RhB concentration in this work. More interestingly, with the increasing of AuNPs concentration ([AuNPs]), the fluorescence intensity of RhB solution was decreased based on the effect of FRET, and the minimum F value was obtained when 0.787 nM AuNPs was added

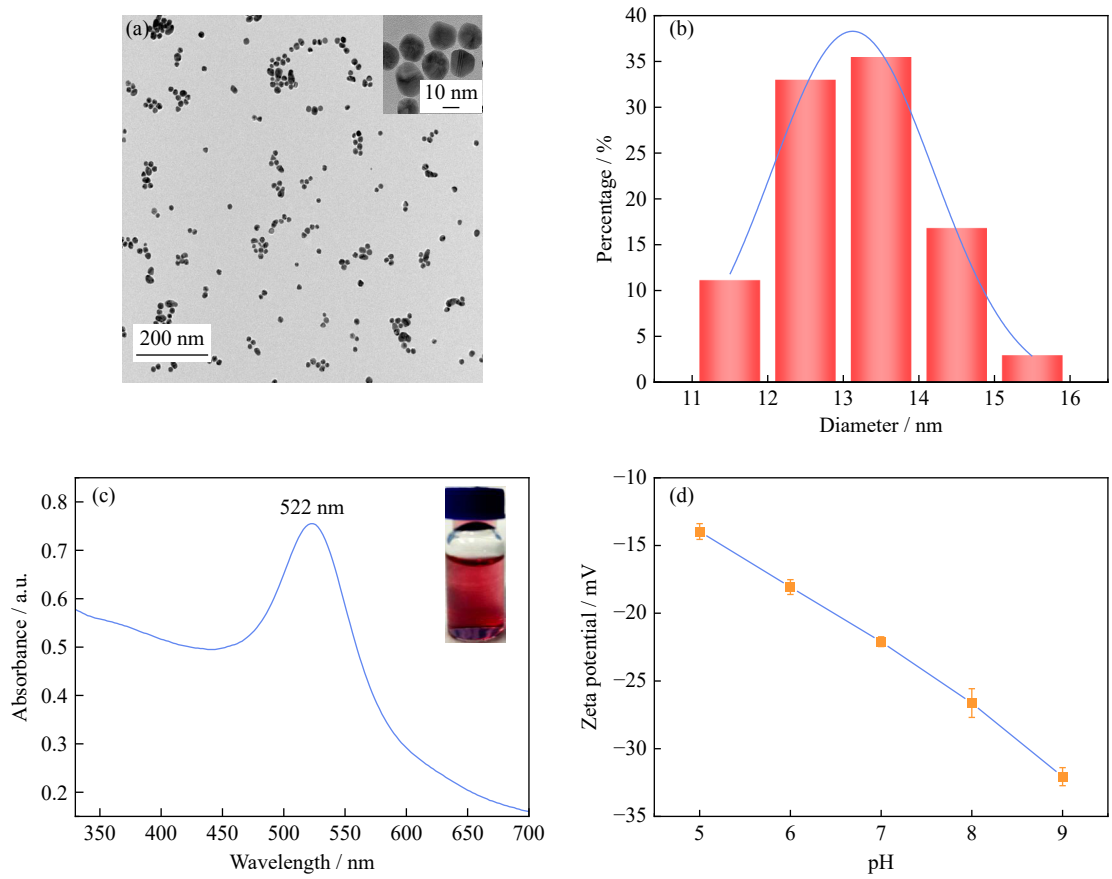

Fig. 2. (a) TEM images and (b) size distribution histogram of AuNPs. (c) Absorption spectrum of AuNPs and (d) zeta potentials of AuNPs dispersed into deionized water at different pH values.

to the RhB solution (Fig. 3(b)). Therefore, the optimal AuNPs concentration was selected as 0.787 nM in the following experiments. Additionally, the effect of the pH value of 0.1 M Tris–HCl buffer solution on the fluorescence response of AuNPs@RhB system was also investigated. As shown in Fig. 3(c), the fluorescence intensity of AuNPs@RhB system also changed slightly with the change of pH from 5 to 9. The maximum response was obtained at the pH = 6 of the 0.1 M Tris–HCl buffer solution. Therefore, the pH = 6 of the 0.1 M Tris–HCl buffer solution was chosen to finish assay. Afterwards, the influence of the incubation time on the Cr^{3+} detection was evaluated. As described in Fig. 3(d), the fluorescence intensity of AuNPs@RhB system was increased with the extension of the reaction time. As described in Fig. 3(d), the fluorescence intensity of AuNPs@RhB system almost remained the same when the incubation time reached 7 min, suggesting that the reaction time of AuNPs and Cr^{3+} reached equilibrium.

3.3. Fluorescence detection of Cr^{3+}

As shown in Fig. 4(a)–(b), the fluorescence intensity of AuNPs@RhB system was increased with the increase of Cr^{3+} concentration ($[Cr^{3+}]$). The liner relationship between the fluorescence intensity of AuNPs@RhB system and Cr^{3+} concentration was shown as $Y = 186.67[Cr^{3+}] + 0.25$, with a correlation coefficient (R^2) of 0.9986, where the F and F_0 were the fluorescence intensities of AuNPs@RhB system in the presence and absence of Cr^{3+}, respectively. Under the optimal conditions, the limit of detection (LOD) for Cr^{3+} was as low as 0.95 nM ($3\sigma/S$, where σ is the standard deviation of blank measurements and S is slope of the calibration curve) with the linear region of 0.164 nM to 3.27 μM. The results showed that the advocated method was excellent for fluorescence detecting Cr^{3+} compared with other methods (as shown in Table 1). Moreover, it was worth noting that the absorbance at 670 nm enhanced gradually as the Cr^{3+} concentration ranging from 0 to 640 nM in the UV–vis absorption spectrum (Fig. 4(c)). A good linear relationship was acquired between I_{630nm}/I_{522nm} and Cr^{3+} concentration (0–640 nM) with $R^2 = 0.9985$, where the I_{630nm} and I_{522nm} were the absorbance values at 630 and 522 nm, respectively. The LOD of Cr^{3+} could be calculated to be 9.76 μM in the colorimetric methods (Fig. 4(d)). Moreover, the above results demonstrated that AuNPs@RhB system was suitable to be applied as a fluorescence probe for the quantitative determination of Cr^{3+}. Therefore, in the UV–vis absorption spectrum, a satisfactory linear relationship could also be obtained with the change of Cr^{3+} concentration, indicating that the proposed fluorescence sensing system could meet the quantitative determination of Cr^{3+} and have certain practical application prospects.

3.4. Selectivity toward Cr^{3+}

Moreover, the validity and selectivity of the promoted fluorescence sensor were researched as shown in Fig. 5. Various potential interfering agents were added into the AuNPs@RhB system under optimal conditions. Fig. 5 re-

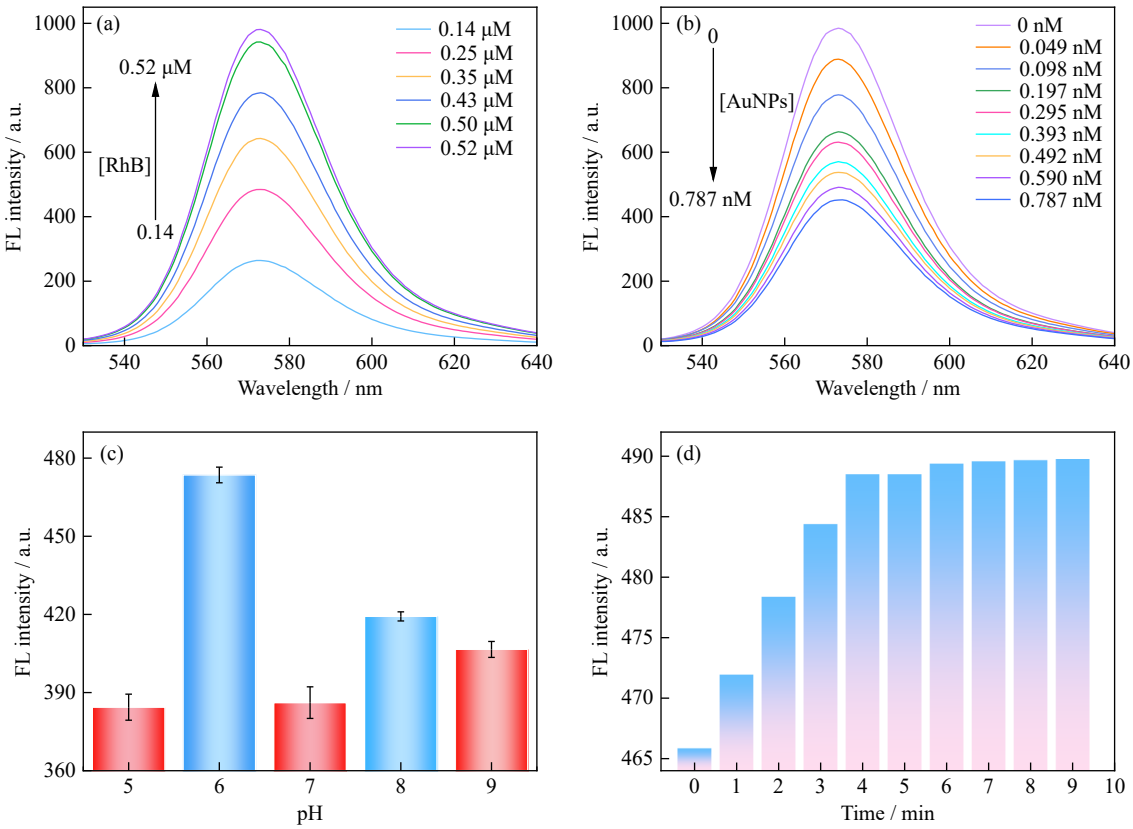

Fig. 3. (a) Fluorescence emission of RhB at different concentrations and (b) fluorescence emission of RhB in the presence of different concentrations of AuNPs. Effect of (c) pH and (d) reaction time on the fluorescence intensity of AuNPs@RhB system in the presence of Cr^{3+} (0.3 μM).

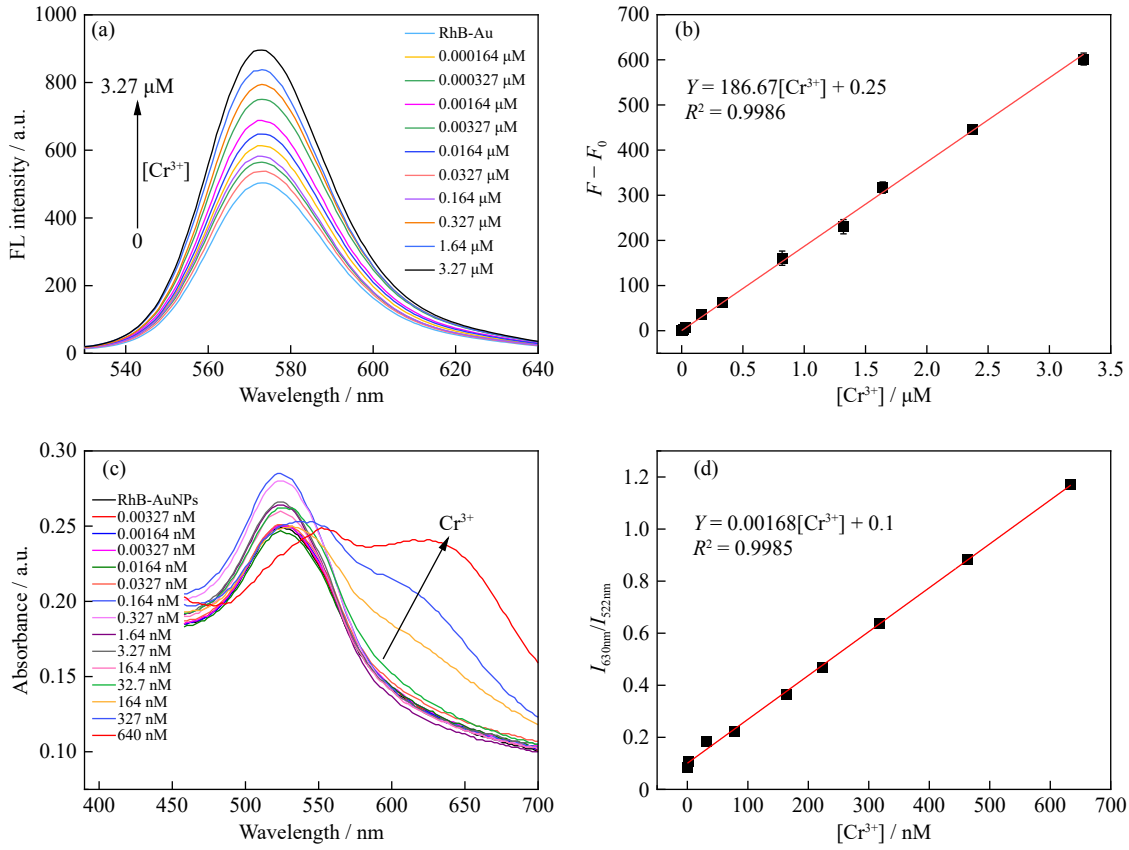

Fig. 4. (a) Fluorescence emission spectra of AuNPs@RhB system in the presence of different Cr^{3+} concentrations. (b) Fitting of linear relationship between ($F - F_0$) and Cr^{3+} concentration. (c) Absorption spectrum of AuNPs@RhB system in the presence of different Cr^{3+} concentrations. (d) Plot of I_{630nm}/I_{522nm} versus Cr^{3+} concentration.

Table 1. Comparison of different methods for Cr^{3+} sensing

Fluorescent probes	Performance		Ref.
	Detection limit / nM	Linear range / μM	
Py-An COF	81700	0–495	[37]
CdTe QDs	3.81	0.05–5	[38]
NBN-embedded polymers	14.69	0–25	[39]
1,2,3-triazolyl-γ-propyltriethoxysilanes	60.6	0–0.6	[40]
JXUST-2	100	0–50	[41]
Cd(II)-MOF	600	0–30	[16]
g-CNQDs	230	0.64–63	[42]
AuNPs@RhB	0.95	0.000164–3.27	This work

veals an excellent selectivity for Cr^{3+} towards other substances, such as Al^{3+}, Na^{+}, Ca^{2+}, Pb^{2+}, Mg^{2+}, Ni^{2+}, Hg^{2+}, K^{+}, Fe^{3+}, Zn^{2+}, Mn^{2+}, Cr^{6+}, Ag^{+}, Cu^{2+}, Co^{2+}, Cd^{2+}, and NH_4^{+}. As depicted in Fig. 5(a), only Cr^{3+} could increase the fluorescence of AuNPs@RhB system, rather than other interfering agents, demonstrating the high selectivity of this fluorescence probe. Interestingly, the AuNPs@RhB system exhibited different color changes in the presence of different substances (insert in Fig. 5(a)), which is possibly due to the aggregation of AuNPs. In addition, to investigate the selectivity of the proposed method, the influence of some possible interfering compounds was also examined through the UV–vis spectroscopy. Based on the results obtained in Fig. 5(b), there was no obvious absorbance peak of the other interfering compounds at 630 nm compared to Cr^{3+}. The Cr^{3+} final concentration was 20 μM. The concentrations of other interferences were about 10-fold than that of Cr^{3+}. Therefore, the proposed fluorescence sensing system was further verified to have high selectivity for Cr^{3+} combined with UV–vis absorption spectra.

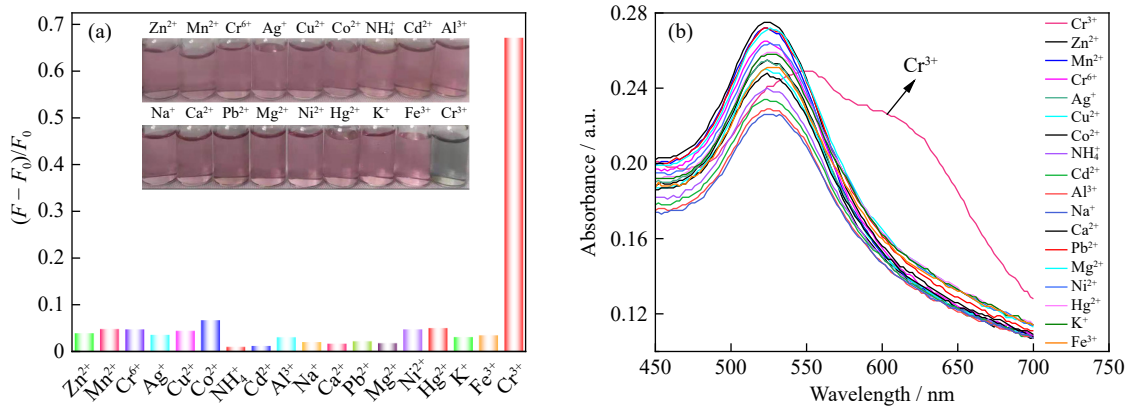

Fig. 5. (a) Fluorescence response and (b) absorption spectrum of the AuNPs@RhB system in the presence of Cr^{3+} and other metal ions.

3.5. Detection of the Cr^{3+} in real samples

In order to prove that the proposed sensing system could be used for the detection of real samples, the fluorescence probe of AuNPs@RhB was used to determine the Cr^{3+} in river water. The concentration of Cr^{3+} in the actual sample was detected by the experiment of labeling and recovery. The results were summarized in Table 2. The results indicated there was a good recovery rate (in the range of 90%–109%) for Cr^{3+} in river water. Hence, it was suggested that the promoted sensing system could be successfully applied to the detection of Cr^{3+} in actual samples.

Table 2. Determination of Cr^{3+} in actual samples by AuNPs@RhB fluorescent probe

Sample	Added Cr^{3+} / μM	Found Cr^{3+} / μM	Recovery (n = 3) / %
River water	0.8	0.72	90
	1.2	1.24	103
	2.0	2.18	109

Note: n means the number of samples.

4. Possible mechanism about sensing of Cr^{3+}

According to the previous experiments, the fluorescence intensity of RhB solution could be intensively quenched by the as-prepared AuNPs. However, it is worth noting that the fluorescence intensity of RhB solution could be obviously increased with the addition of Cr^{3+} to the AuNPs@RhB system. Therefore, to elucidate the possible detection mechanism of this sensor, the fluorescence spectra of RhB and the UV–vis spectra of AuNPs were taken and analyzed (Fig. 6). The UV–vis absorption spectrum of AuNPs (blue line) and the fluorescence emission spectrum of RhB (yellow line) were shown in Fig. 6. It was obvious that the fluorescence emission spectrum (yellow line) of RhB greatly overlapped with the absorption spectrum (blue line) of AuNPs to an extent,

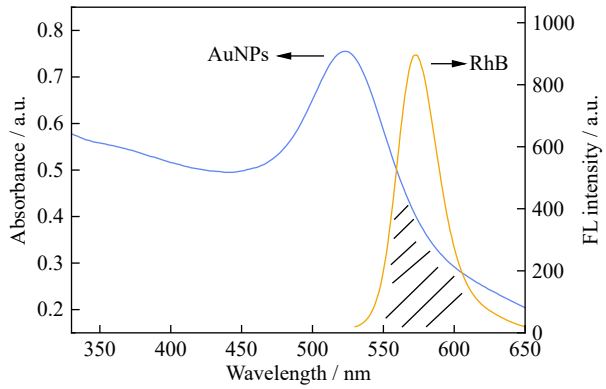

Fig. 6. Absorption spectrum of AuNPs (blue line) and fluorescence emission spectrum of RhB (yellow line).

suggesting that FRET might take place between RhB (as donor) and AuNPs (as acceptor). This phenomenon was also proved by the decrease of the fluorescence intensity of RhB with the increase of AuNPs concentration.

Additionally, the TEM images of AuNPs@RhB system after adding a certain amount of Cr^{3+} were measured to investigate the reason of the recovery of the fluorescence intensity of RhB. From the Fig. 7(a) and (b), the TEM images exhibited a significant aggregation of AuNPs@RhB driven by Cr^{3+} ion. Moreover, to further prove the detection mechanism of AuNPs@RhB system for Cr^{3+}, the absorption spectrum of the AuNPs@RhB (purple line), AuNPs@RhB in the presence of Cr^{3+} (yellow line), and only Cr^{3+} (blue line) were performed in Fig. 7(c). Compared with AuNPs, the spectrum of Cr^{3+} solution had a weaker adsorption peak at 575 nm. However, upon addition of Cr^{3+}, the adsorption peak of AuNPs@RhB exhibited a red-shift and appeared a new absorption peak at 630 nm. At this moment, the color of AuNPs@RhB solution immediately turned to black (Fig. 7(d)). Therefore, the reason for the recovery of fluorescence intensity of the proposed sensing system might be due to the strong interaction of Cr^{3+} with specific groups on the surface of citrate stabilized AuNPs, causing AuNPs to aggregate. The color of the reaction solution turned to black after adding Cr^{3+}, and the fluorescence intensity of the advocated system was further restored.

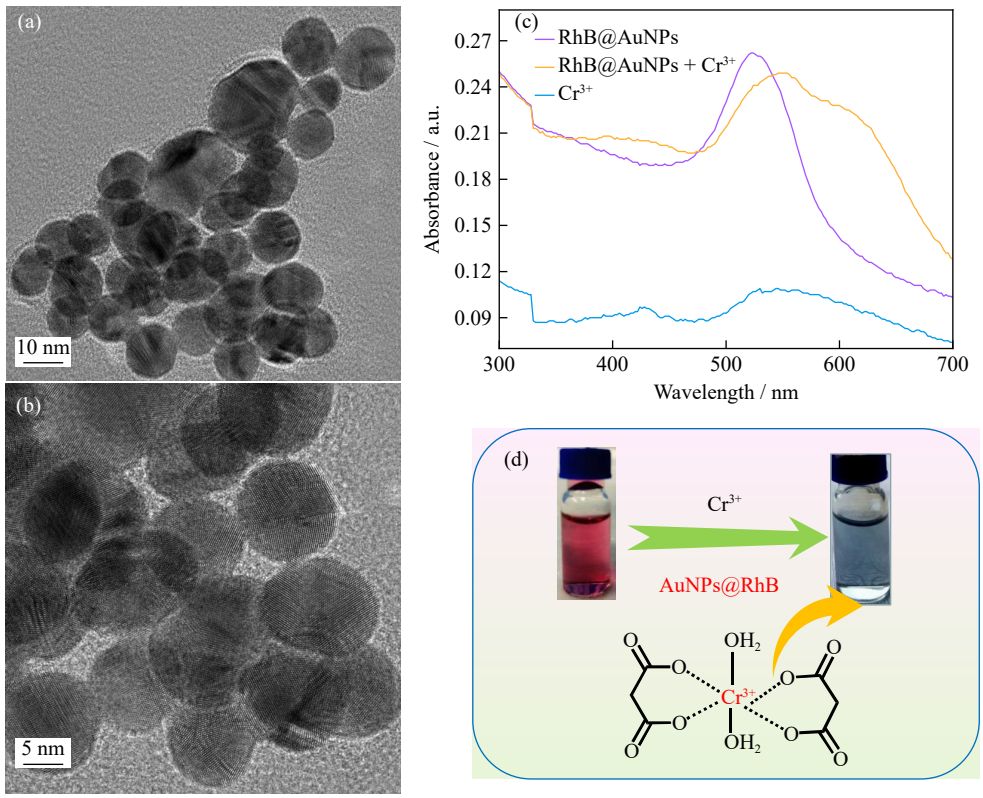

Fig. 7. (a, b) TEM images for AuNPs@RhB system after addition of Cr^{3+}. (c) Absorption spectrum of the AuNPs@RhB (purple line), AuNPs@RhB in the presence of Cr^{3+} (yellow line), and only Cr^{3+} (blue line). (d) Possible mechanism about sensing of Cr^{3+}.

5. Conclusion

In summary, a novel fluorescence and colorimetric sensor for Cr^{3+} was proposed using AuNPs@RhB probe. Upon addition of Cr^{3+} to AuNPs@RhB system, fluorescence intensity was recovered based on the complexation between the specific groups on the surface of citrate-stabilized AuNPs and Cr^{3+}, resulting the aggregation of AuNPs. Based on the view above, the assay proved that this method displayed several advantages of high sensitivity, excellent selectivity, simplicity, and non-time consuming with a detection limit of 0.95 nM. Overall, this work will open up a new insight into the application of AuNPs@RhB system in sensing Cr^{3+} in environment.

Acknowledgements

This work was supported by the Natural Science Founda-

tion of Qinghai Province in China (No. 2019-ZJ-944Q) and the University-level Planning Project of Qinghai Minzu University of Qinghai Province in China (Nos. 2022GH11 and 2022GH13).

Conflict of Interest

The authors declare that they have no known competing financial interests or personal relationships that could have appeared to influence the work reported in this paper.

References

[1] K. Al-Hamoud, M.R. Shaik, M. Khan, *et al.*, *Pulicaria undulata* extract-mediated eco-friendly preparation of TiO_2 nanoparticles for photocatalytic degradation of methylene blue and methyl orange, *ACS Omega*, 7(2022), No. 6, p. 4812.

[2] X.R. Chen, W.R. Cui, R.P. Liang, *et al.*, Band gap engineering in vinylene-linked covalent organic frameworks for enhanced photocatalytic degradation of organic contaminants and disinfection of bacteria, *ACS Appl. Bio Mater.*, 4(2021), No. 8, p. 6502.

[3] Y.L. Chen, X. Bai, Y.T. Ji, and D.D. Chen, Enhanced activation of peroxymonosulfate using ternary MOFs-derived MnCoFeO for sulfamethoxazole degradation: Role of oxygen vacancies, *J. Hazard. Mater.*, 441(2023), art. No. 129912.

[4] Z.M. Fang, Y.B. Liu, J.J. Qi, Z.F. Xu, T.Y. Qi, and L.D. Wang, Establishing a high-speed electron transfer channel via CuS/MIL-Fe heterojunction catalyst for photo-Fenton degradation of acetaminophen, *Appl. Catal. B*, 320(2023), art. No. 121979.

[5] B.F. Zhang, L. Zhang, K. Akiyama, P.A. Bingham, Y.T. Zhou, and S. Kubuki, Self-assembly of nanosheet-supported Fe-MOF heterocrystals as a reusable catalyst for boosting advanced oxidation performance via radical and nonradical pathways, *ACS Appl. Mater. Interfaces*, 13(2021), No. 19, p. 22694.

[6] K.Z. Zhang, X.Y. Tian, P.P. Xu, Y. Zhu, S.Y. Guang, and H.Y. Xu, Multi-ion detection chemosensor based on rhodamine for turn-on fluorescence sensing and bioimaging of Fe^{3+}, Al^{3+}, Cr^{3+}, and Hg^{2+} under different channels, *Spectrochim. Acta Part A*, 318(2024), art. No. 124484.

[7] J.Y. Qu, D.P. Zhang, Y.X. Li, *et al.*, *In situ* synthesized S-type heterojunction $Bi_2O_2CO_3/CuBi_2O_4$ enable efficient NIR light-driven H_2O_2 activation for water purification, *Appl. Catal. B*, 340(2024), art. No. 123246.

[8] M.L. Liu, S.T. Zhang, Y.S. Wang, J. Liu, W.P. Hu, and X.Q. Lu, Hexavalent chromium as a smart switch for peroxidase-like activity regulation via the surface electronic redistribution of silver nanoparticles anchored on carbon spheres, *Anal. Chem.*, 94(2022), No. 3, p. 1669.

[9] D. Promrug, D. Arthan, and P. Thongyoo, Development of a fluorescent sensor for dual visual detection of Cr^{3+} and H_2S using a fluorescein framework and bio-imaging applications, *Microchem. J.*, 205(2024), art. No. 111323.

[10] R. Meena, V.N. Mehta, J.R. Bhamore, P.T. Rao, T.J. Park, and S.K. Kailasa, Diaminodiphenyl sulfone as a novel ligand for synthesis of gold nanoparticles for simultaneous colorimetric assay of three trivalent metal cations (Al^{3+}, Fe^{3+} and Cr^{3+}), *J. Mol. Liq.*, 312(2020), art. No. 113409.

[11] E. Dhineshkumar, M. Iyappan, and C. Anbuselvan, A novel dual chemosensor for selective heavy metal ions Al^{3+}, Cr^{3+} and its applicable cytotoxic activity, HepG2 living cell images and theoretical studies, *J. Mol. Struct.*, 1210(2020), art. No. 128033.

[12] C.L. He, Y. Liu, M.W. Qi, *et al.*, A functionalized activated carbon adsorbent prepared from waste amidoxime resin by modifying with H_3PO_4 and $ZnCl_2$ and its excellent Cr(VI) adsorption, *Int. J. Miner. Metall. Mater.*, 31(2024), No. 3, p. 585.

[13] P. Zhang, X. Xu, Y.F. Cui, X.H. Wei, S.J. Memg, and Y.X. Sun, A highly sensitive and selective bissalamo-coumarin-based fluorescent chemical sensor for Cr^{3+}/Al^{3+} recognition and continuous recognition S^{2-}, *J. Photochem. Photobiol. A*, 408(2021), art. No. 113066.

[14] K. Çevik, İ. Yildiz, A. Yildiz, M.S. Nas, M.H. Alma, and M.H. Calimli, $PdRuO_2$/PVP nanomaterial as a highly selective, stable, and applicable potentiometric sensor for the detection of Cr^{3+}, *Microchim. Acta*, 191(2024), No. 8, art. No. 467.

[15] S. Al-Sodies, A.M. Asiri, M.M. Alam, K.A. Alamry, M.A. Hussein, and M.M. Rahman, Sensitive Cr^{3+} sensor based on novel poly(luminol-co-1, 8-diaminonaphthalene)/CeO_2/MWCNTs nanocomposites, *RSC Adv.*, 14(2024), No. 9, p. 5797.

[16] T. Wiwasuku, J. Boonmak, R. Burakham, *et al.*, Turn-on fluorescent probe towards glyphosate and Cr^{3+} based on Cd(II)-metal organic framework with Lewis basic sites, *Inorg. Chem. Front.*, 8(2021), No. 4, p. 977.

[17] P.L. Abreu, T. Cunha-Oliveira, L.M.R. Ferreira, and A.M. Urbano, Hexavalent chromium, a lung carcinogen, confers resistance to thermal stress and interferes with heat shock protein expression in human bronchial epithelial cells, *Biometals*, 31(2018), No. 4, p. 477.

[18] S. Sangsin, P. Srivilai, and P. Tongraung, Colorimetric detection of Cr^{3+} in dietary supplements using a smartphone based on EDTA and tannic acid-modified silver nanoparticles, *Spectrochim. Acta Part A*, 246(2021), art. No. 119050.

[19] Q.Y. Yang, C.Q. Wan, Y.X. Wang, X.F. Shen, and Y.H. Pang, Bismuth-based metal-organic framework peroxidase-mimic nanozyme: Preparation and mechanism for colorimetric-converted ultra-trace electrochemical sensing of chromium ion, *J. Hazard. Mater.*, 451(2023), art. No. 131148.

[20] X.M. Li, S.T. Zhang, Y.F. Dang, *et al.*, Ultratrace naked-eye colorimetric ratio assay of chromium(III) ion in aqueous solution via stimuli-responsive morphological transformation of silver nanoflakes, *Anal. Chem.*, 91(2019), No. 6, p. 4031.

[21] R. Tamizhselvi and A.A. Napoleon, Ninhydrin and isatin appended 2-hydrazinobenzothiazole based simple Schiff bases for colorimetric selective detection of Cr^{3+} and Pb^{2+} ions, *Inorg. Chem. Commun.*, 145(2022), art. No. 109983.

[22] W.Z. Lin, C.Y. Yeung, C.K. Liang, Y.H. Huang, C.C. Liu, and S.Y. Hou, A colorimetric sensor for the detection of hydrogen peroxide using DNA-modified gold nanoparticles, *J. Taiwan Inst. Chem. Eng.*, 89(2018), p. 49.

[23] H.B. Chen, Y. Luo, W.R. Cai, L.D. Xu, J.Y. Li, and Y. Kong, Colorimetric discrimination and spectroscopic detection of tyrosine enantiomers based on melamine induced aggregation of L-cysteine/Au nanoparticles, *Talanta*, 271(2024), art. No. 125758.

[24] A. Khitous, L. Noel, C. Molinaro, L. Vidal, S. Grée, and O. Soppera, Sol–gel TiO_2 thin film on Au nanoparticles for heterogeneous plasmonic photocatalysis, *ACS Appl. Mater. Interfaces*, 16(2024), No. 8, p. 10856.

[25] K.X. Li, H. Li, Q. Zhang, D.Z. Yang, and Y.L. Yang, Core–shell structure DA-CDs/AuNPs for the recognition of fenamidone by surface-enhanced Raman scattering, *Spectrochim. Acta Part A*, 310(2024), art. No. 123865.

[26] W.F. Jia, J.R. Li, and L. Jiang, Synthesis of highly branched gold nanodendrites with a narrow size distribution and tunable NIR and SERS using a multiamine surfactant, *ACS Appl. Mater. Interfaces*, 5(2013), No. 15, p. 6886.

[27] Z.N. Liu, L.C. Liu, J.P. Xue, S.G. Li, and X. Li, Ultrasensitive L-methionine functionalized AuNPs for colorimetric and UV–vis dual-mode parallel detection of As^{3+}, Cd^{2+} and Hg^{2+}, *J. Nanopart. Res.*, 26(2024), No. 5, art. No. 84.

[28] H.Y. Xi, W.W. He, Q.Y. Liu, and Z.B. Chen, Protein discrimination using a colorimetric sensor array based on gold nanoparticle aggregation induced by cationic polymer, *ACS Sustainable Chem. Eng.*, 6(2018), No. 8, p. 10751.
[29] W.G. Zhang, X.F. Zhu, M.X. Kang, *et al*., Water splitting-assisted electrocatalysis based on dendrimer-encapsulated Au nanoparticles for perspiration glucose analysis, *J. Electroanal. Chem.*, 912(2022), art. No. 116254.
[30] A.S. Andreani, E.S. Kunarti, T. Hashimoto, T. Hayashita, and S.J. Santosa, Fast and selective colorimetric detection of Fe^{3+} based on gold nanoparticles capped with ortho-hydroxybenzoic acid, *J. Environ. Chem. Eng.*, 9(2021), No. 5, art. No. 105962.
[31] Q. Zhao, Q.L. Zhang, C. Du, *et al*., Synergistic effect of dual particle-size AuNPs on TiO_2 for efficient photocatalytic hydrogen evolution, *Nanomaterials*, 9(2019), No. 4, art. No. 499.
[32] L.L. Sun, W.L. Wei, H.M. Zhang, J.Y. Xu, and X.H. Zhao, A simple colorimetric and fluorescent "on-off-on" dual-mode sensor based on cyan fluorescent carbon dots/AuNPs for the detection of L-cysteine and Zinc thiazole, *Microchem. J.*, 174(2022), art. No. 107079.
[33] H.W. Xiong, Z.P. Huang, Q.Y. Lin, *et al*., Surface plasmon coupling electrochemiluminescence immunosensor based on polymer dots and AuNPs for ultrasensitive detection of pancreatic cancer exosomes, *Anal. Chem.*, 94(2022), No. 2, p. 837.
[34] Q.L. Wang, L.C. Liu, X.Y. Chen, *et al*., Noninvasive prognosis of postmyocardial infarction using urinary miRNA ultratrace detection based on single-target DNA-functionalized AuNPs, *ACS Appl. Mater. Interfaces*, 14(2022), No. 3, p. 3633.
[35] I. Ojea-Jiménez, F.M. Romero, N.G. Bastús, and V. Puntes, Small gold nanoparticles synthesized with sodium citrate and heavy water: Insights into the reaction mechanism, *J. Phys. Chem. C*, 114(2010), No. 4, p. 1800.
[36] L. Dong, C.J. Hou, H.B. Fa, *et al*., Highly sensitive fluorescent sensor for cartap based on fluorescence resonance energy transfer between gold nanoparticles and rhodamine B, *J. Nanosci. Nanotechnol.*, 18(2018), No. 4, p. 2441.
[37] S.J. Qiao, J.W. Wang, and Z.Y. Guo, Ratiometric fluorescent detection of chromium(III) based on one-dimensional imine-linked covalent organic framework, *Inorg. Chem.*, 63(2024), No. 1, p. 706.
[38] X.T. Wu, L. Tan, Y.L. Li, *et al*., Novel sensor array distinguishes heavy metal ions based on multiple fluorescence channels from dendritic mesoporous silica nanoparticles, *Anal. Chim. Acta*, 1240(2023), art. No. 340749.
[39] T. Li, Y.J. Sheng, X.L. Sun, *et al*., Novel NBN-embedded polymers and their application as fluorescent probes in Fe^{3+} and Cr^{3+} detection, *Polymers*, 14(2022), No. 10, art. No. 2025.
[40] G. Singh, A. Devi, Mohit, *et al*., Development of piperazine conjoined 1,2,3-triazolyl-γ-propyltriethoxysilanes: Fluorometric detection of Cr^{3+} ions and computational study, *Spectrochim. Acta Part A*, 291(2023), art. No. 122358.
[41] X.M. Tian, S.L. Yao, C.Q. Qiu, *et al*., Turn-on luminescent sensor toward Fe^{3+}, Cr^{3+}, and Al^{3+} based on a Co(II) metal-organic framework with open functional sites, *Inorg. Chem.*, 59(2020), No. 5, p. 2803.
[42] X.H. Xu, H.Y. Li, Y.P. Sun, *et al*., Novel "on–off" fluorescence sensing for rapid and accurate determination of Cr^{3+} based on g-CNQDs, *RSC Adv.*, 13(2023), No. 41, p. 28550.